Extended-Hückel-theory calculation of hyperfine interactions of the positive divacancy in silicon

C A J Ammerlaan† and C Weigel‡

† Natuurkundig Laboratorium, Universiteit van Amsterdam, Valckenierstraat 65, Amsterdam, The Netherlands

‡ Physics Department, State University of New York at Albany, Albany, New York 12222, USA

Abstract. Using extended Hückel theory, an LCAO–MO wavefunction was calculated for the unpaired electron of the positive divacancy in silicon. Calculations were carried out in the molecular unit cell approach for the Γ point. The unit cell of the periodic array was a 62 atom cluster, that is, a 64 atom perfect cell with two atoms removed to form the divacancy. The unpaired divacancy electron occupies a level of symmetry type B_u, which is located in the valence band near the band edge. From the wavefunction, expressed in Slater-type 3s and 3p atomic orbitals, the hyperfine interactions of the defect electron with ^{29}Si nuclei surrounding the divacancy were obtained. A systematic study was made of the effects of Jahn–Teller deformations of the six nearest-neighbour atoms of the divacancy, for the two distortion modes which reduce the trigonal symmetry of the defect to monoclinic. Also, the effects of symmetric relaxation of the nearest neighbours, and of relaxation of the next-nearest-neighbour atoms were considered. Results for the tensors calculated were compared with the tensors determined experimentally by electron–nuclear double resonance. Good agreement is obtained for the two shells containing the nearest-neighbour atoms. The identification made for the general class tensor is, however, different from an interpretation based on a motional-averaging experiment. For the five shells containing the 18 next-nearest-neighbour atoms, only some tentative tensor assignments can be suggested. Assignments of hyperfine tensors to specific shells of atoms is generally based upon agreement for the isotropic part of the interaction and for the principal values of the axial part of the dipole–dipole interaction. For the direction of this axis and for the deviations from axial symmetry often a bad match is obtained.

1. Introduction

In an attempt to improve the understanding of the electronic structure of deep-level defects in semiconductors, calculations were performed for the divacancy in silicon. These calculations yielded electron energy levels, wavefunctions, and hyperfine interaction constants. The divacancy in silicon, in its positive charge state, was chosen for this study because for this defect, detailed information on the hyperfine interactions with ^{29}Si nuclei is available from electron–nuclear double resonance measurements (De Wit *et al* 1975, 1976). Though extended Hückel theory (EHT) (Hoffmann 1963, Messmer and Watkins 1970, 1973a) is only a semi-empirical method, it was applied in the present calculations. Our justification for this choice is that EHT has been shown to yield reasonable, if not good, results for the description of the electronic properties of defects in various covalent solids. Moreover, the calculation of hyperfine interactions with distant nuclei requires a spatially extended wavefunction. Simple EHT allows the use of a large-basis set of atomic orbitals, in contrast to more exact theories, like the defect-molecule method or SCF-SW-Xα.

2. Details of the calculation

2.1. *Atomic orbitals*

The basic functions in which the electron wavefunction is expressed are normalized Slater-type atomic orbitals:

$$\chi_{3s} = N_s r^2 \exp(-\alpha_s r) \qquad \text{with} \qquad N_s^2 = 2\alpha_s^7/45\pi, \tag{1}$$

$$\chi_{3px} = N_p\, xr \exp(-\alpha_p r) \qquad \text{with} \qquad N_p^2 = 2\alpha_p^7/15\pi, \tag{2}$$

etc. Our values for the orbital exponents, $\alpha_s = 1{\cdot}87$ and $\alpha_p = 1{\cdot}60$, are equal to those of Messmer and Watkins (Messmer 1975), but differ from the choice of others (Kwok 1974).

2.2. *Symmetry orbitals*

To reduce the computational labour symmetry, adapted orbitals were projected out:

$$\sigma_a = \sum_\mu d_{\mu a}\chi_\mu .$$

This, at the same time, implies grouping the atoms around the defect in shells. Two classes of shell exist: mirrorplane shells and general shells. The symmetry orbitals are basis functions of the irreducible representations A_g, A_u, B_g, or B_u of the point group $C_{2h}(2/m)$ which is the experimentally observed symmetry of the divacancy. The one-electron molecular orbitals ϕ_i are constructed as linear combinations of these symmetry orbitals σ_a:

$$\phi_i = \sum_a c_{ai}\,\sigma_a = \sum_a c_{ai}\Big(\sum_\mu d_{\mu a}\chi_\mu\Big) \equiv \sum_\mu c'_{\mu i}\,\chi_\mu . \tag{3}$$

2.3. *Molecular unit cell approach*

To eliminate the spurious levels due to dangling bonds on the surface, the molecular unit cell approach (Messmer and Watkins 1973b, Lee and McGill 1973) was adopted. A (62 atom + V_2) unit cell was repeated periodically. The unit cell consisted of a cubic block of two by two by two face-centred-cubic cells, with two atoms in the centre removed to form the divacancy. Calculations were only performed for the Γ point. For this particular point in k space the Bloch sums $\psi_{\Gamma,i}$ are given by:

$$\psi_{\Gamma,i} = N^{-1/2}\sum_{l=1}^{N} \phi_i(\mathbf{r}-\mathbf{R}_l) \tag{4}$$

where the $\mathbf{R}_l$ represent the translation vectors of the simple cubic lattice. Its lattice parameter was taken to be equal to 10·858 Å.

2.4. *Extended Hückel theory*

The one-electron energies E_i and the corresponding wavefunctions are obtained by equating the secular determinant $|H_{ab\Gamma} - E_i S_{ab\Gamma}|$ to zero and solving the system of linear equations

$$\sum_a (H_{ab\Gamma} - E_i S_{ab\Gamma})\, c_{ai} = 0$$

for the coefficients c_{ai}. The interaction integrals $H_{ab\Gamma}$ and overlap integrals $S_{ab\Gamma}$ can be reduced to integrals involving atomic orbitals only. Overlap integrals were evaluated analytically. Interaction integrals are obtained via the Wolfsberg–Helmholtz approximation: $H_{\mu\nu} = -\tfrac{1}{2} K_{\mu\nu}(I_\mu + I_\nu) S_{\mu\nu}$. For orbitals on the same site $K_{\mu\nu} = 1$; for orbitals on different sites $K_{\mu\nu}$ has the empirically determined values $K_{ss} = K_{pp} = 1{\cdot}75$, and $K_{sp} = 1{\cdot}313$. I_s and I_p are the atomic ionization energies, and in our calculations the values $I_s = 14{\cdot}95$ eV and $I_p = 7{\cdot}77$ eV were used.

2.5. *Hyperfine tensor components*

From the wavefunction of the unpaired divacancy electron the hyperfine interaction with ^{29}Si nuclei on all lattice sites around the defect can be calculated. First, to avoid singularities in the integrals, the s-part of the wavefunction on the hyperfine site is separated. Contact interaction arising from the 3s atomic orbitals, with its centre on the hyperfine site is calculated using a probability density $|\psi_{3s}(0)|^2 = 31{\cdot}5 \times 10^{24}\,\mathrm{cm}^{-3}$ from Watkins and Corbett (1964). Dipole–dipole tensor components were obtained from the expression:

$$B_{\alpha\beta} = g_e \mu_B g_N \mu_N \langle\phi_i|(3r_\alpha r_\beta - r^2\delta_{\alpha\beta})/r^5|\phi_i\rangle, \tag{5}$$

with $\alpha, \beta = x, y, z$, and all other symbols having their usual meaning. After substitution of

$$\phi_i = \sum_\mu c'_{\mu i} \chi_\mu$$

expression (5) may be decomposed into

$$B_{\alpha\beta} = B^{\mathrm{I}}_{\alpha\beta} + 2\sum_{j\neq 1} B^{\mathrm{II}}_{\alpha\beta} + \sum_{j\neq 1} B^{\mathrm{III}}_{\alpha\beta} + \sum\sum_{1\neq i\neq j\neq 1} B^{\mathrm{IV}}_{\alpha\beta}. \tag{6}$$

The summations in equation (6) are over lattice sites, where the ^{29}Si hyperfine site carries index 1. The first term on the right-hand side of equation (6) takes account of the atomic orbitals centred on the ^{29}Si site. Its evaluation leads to the familiar axially symmetric interaction, with $b = \tfrac{2}{5}(g_e \mu_B g_N \mu_N)\langle r^{-3}\rangle_{3p}$. For $\langle r^{-3}\rangle_{3p}$ we took $16{\cdot}1 \times 10^{24}\,\mathrm{cm}^{-3}$ (Watkins and Corbett 1964). When only one of the atomic orbitals is centred on the hyperfine site the terms $B^{\mathrm{II}}_{\alpha\beta}$ describe the interaction. Terms $B^{\mathrm{III}}_{\alpha\beta}$ account for the hyperfine interaction when both orbitals have a common centre, which is however different from the ^{29}Si site. The terms $B^{\mathrm{II}}_{\alpha\beta}$ and $B^{\mathrm{III}}_{\alpha\beta}$ involve two-centre integrals, for which analytical expressions could be derived (C A J Ammerlaan and J C Wolfrat, unpublished). Finally, when both atomic orbitals and the hyperfine nucleus have no centre in common, the terms $B^{\mathrm{IV}}_{\alpha\beta}$ require the evaluation of three-centre integrals. Contributions from these last terms are likely to be small and were therefore neglected.

The calculated tensors were transformed to their principal axes systems. It was found convenient to equate the principal values in order of descending magnitude to $a + 2b$, $a - b + c$, and $a - b - c$, respectively. The parameter a then describes the isotropic or contact interaction. The purely axial part is given by b, while c takes account of deviations from axial symmetry.

3. Results and discussion

3.1. Energy levels

A first topic to be considered is the distribution of electrons over the eigenstates. For this purpose figure 1 shows the energy levels which are located near the bandgap. For reference the energy positions for the bottom of the conduction band at $E_c = -6{\cdot}67$ eV, and for the top of the valence band at $E_v = -7{\cdot}75$ eV are included in the figure. These values were taken from an EHT bandstructure calculation using identical parameters as for the calculation for the solid with the defect. With the divacancy in the positive charge charge state a 62-atom unit cell contains 247 electrons. If these electrons are put into the lowest possible levels, which represents the most straightforward way of filling, three electrons are left for the levels labelled $A_u(1)$ and $B_u(1)$. The unpaired electron occupies a level located in the valence band, while it should have been in the bandgap. Clearly, the energies of the electron states associated with the divacancy are predicted too low by EHT. The situation is reminiscent of the surface dangling-bond states. The

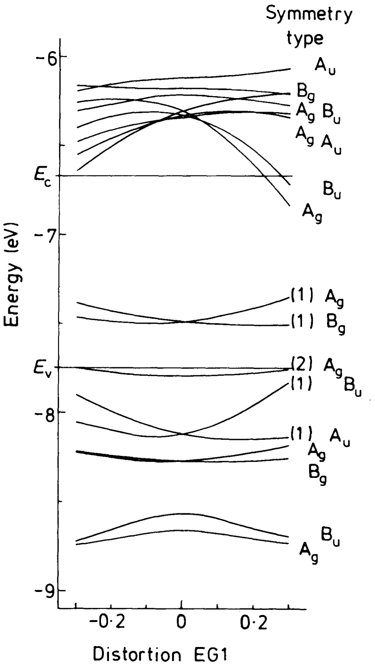

Figure 1. Energies of the one-electron molecular orbitals near the bandgap as functions of the distortion parameter EG1. All other distortion parameters are zero.

problem may be remedied by artificially lifting the states $A_u(1)$ and $B_u(1)$ into the bandgap. Probably no such problems arise with level $A_g(2)$. This is a state having a low localization on the divacancy, showing almost no sensitivity to distortions around the defect, and is therefore more like a valence-band state. Its energy is likely to be predicted more reliably with respect to the valence-band edge. An alternative way of filling energy states therefore suggests itself. In this recipe the level $A_g(2)$ obtains two electrons first, leaving only one electron for the levels $A_u(1)$ and $B_u(1)$. The unpaired electron will then be in the lowest of these two levels. We have preferred the latter procedure for electron distribution.

3.2. Nearest-neighbour distortions

From the discussion in the previous section it follows that the highest electron will occupy an orbitally degenerate E_u type level for zero distortion, EG1 = 0. It is known from the Hellmann–Feynman theorem that the system may lower its energy by a spontaneous distortion, thereby lowering the symmetry and lifting the degeneracy. The resulting symmetry for the divacancy in silicon from EPR is known to be C_{2h}. Considering only displacements of the six nearest neighbours there exist 18 degrees of freedom for distortions. Only two of these, however, lead to the required C_{2h} symmetry. These two distortion modes, designated by EG1 and EG2, are shown in figure 2. One unit distortion is defined as an RMS displacement of the six nearest-neighbour atoms of 1 Å. Also included in figure 2 are sketches of the two symmetric relaxation modes AG1 and AG2. The picture of AG1 also serves the purpose of defining the coordinate system. Atoms (1, 3, 3) and ($\bar{1}$, $\bar{3}$, $\bar{3}$) constitute the nearest-neighbour mirrorplane shell.

3.3. The distortion modes EG1 and EG2

Computations of the hyperfine parameters *a*, *b* and *c*, and also of angles γ_i and δ_i, (i = 1–3, specifying the direction of the principal axes) were performed systematically

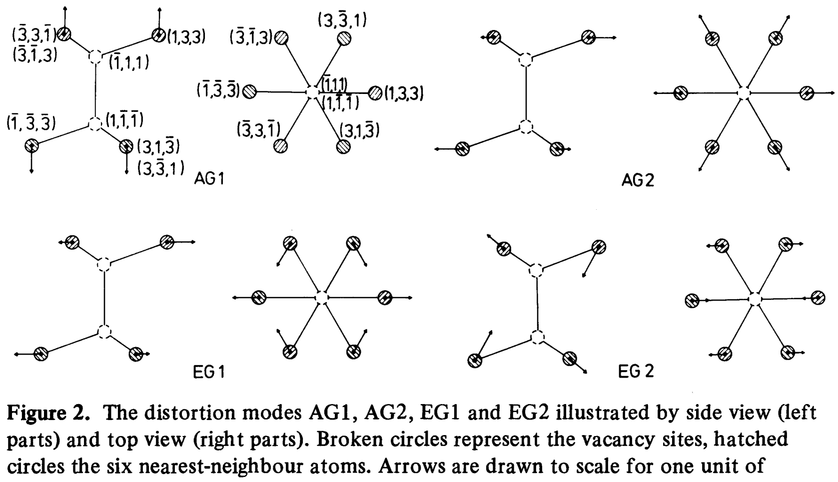

Figure 2. The distortion modes AG1, AG2, EG1 and EG2 illustrated by side view (left parts) and top view (right parts). Broken circles represent the vacancy sites, hatched circles the six nearest-neighbour atoms. Arrows are drawn to scale for one unit of distortion.

over the region $-0{\cdot}3 \leqslant \mathrm{EG1}, \mathrm{EG2} \leqslant 0{\cdot}3$, in steps of 0·1 for both the distortion parameters. The results for several states, which have their energy near the bandgap, and also show a high degree of localization on the divacancy neighbours, were compared with data known from experiment. It is clear at the outset that MOs of symmetry-type $\mathrm{A_u}$ and $\mathrm{B_g}$ can be left out of consideration, since their wavefunctions have a nodal plane on the reflection plane of the divacancy, and they consequently predict a zero value for the contact interaction of mirrorplane class tensors. This would obviously contradict experimental findings. At this stage the results for nearest-neighbour shells were the only ones considered, by comparing the (1, 3, 3) shell results with tensor M1, and the $(\bar{3}, 3, \bar{1})$ shell results with the largest general class tensors. Among the $\mathrm{A_g}$- and $\mathrm{B_u}$-type molecular orbitals there appears to be only one possible candidate for the unpaired electron to be accommodated in; this no doubt is the $\mathrm{B_u}$ (1) level. For this particular level a summary of the results is shown in figure 3. The heavy line in the figure separates the (EG1, EG2) plane in two parts. In the upper left part the unpaired electron occupies the $\mathrm{B_u}(1)$ level, according to the second method of filling states described. For the other way of distributing electrons over states, the regions for occupation of $\mathrm{A_u}$ and $\mathrm{B_u}$ would be simply reversed. The other curves in the figure represent the (EG1, EG2) pairs for which agreement, or best agreement, exists between the calculated (1, 3, 3) shell tensor components and M1 (full curves), and the $(\bar{3}, 3, \bar{1})$ shell compared with G1 or G2 (broken curves). Obviously the lines do not pass through one point, as they should for the perfect theory. However, there are regions of promising combinations, especially for (EG1, EG2) near (0·15, 0·1). More detailed results for the two nearest-neighbour shells for a trajectory given by EG1 + EG2 = 0·2 are presented in figures 4 and 5.

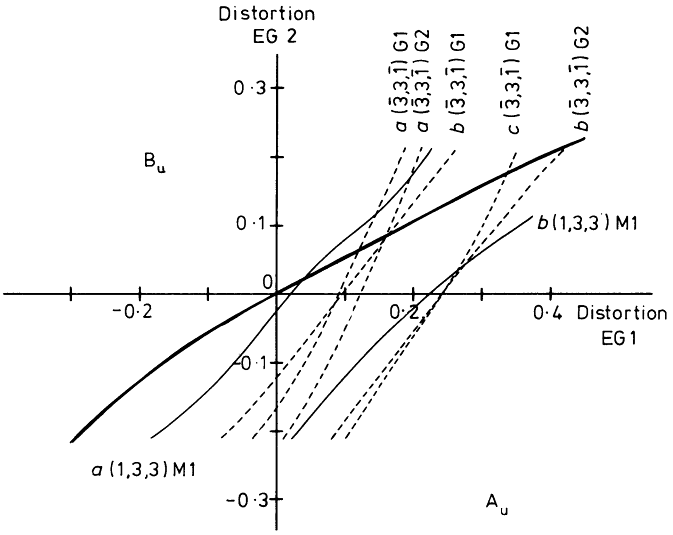

Figure 3. Division of the (EG1, EG2) plane for lowest-lying $\mathrm{A_u}$ or $\mathrm{B_u}$ level, together with curves representing a best match between calculated and measured hyperfine parameters *a*, *b* and *c*. Labels to the curves specify the relevant shell and tensor.

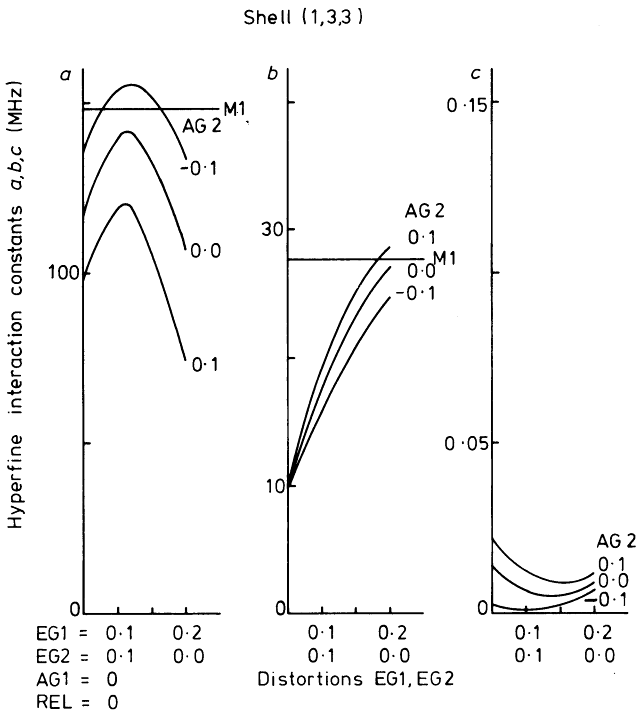

Figure 4. Computed results for the hyperfine interaction constants *a*, *b* and *c* for the nearest-neighbour mirrorplane shell (1, 3, 3) for some (EG1, EG2) combinations satisfying EG1 + EG2 = 0·2. The breathing-mode parameter AG2 is given as label to the curves. AG1 and REL are zero. Experimental values for M1 from Watkins and Corbett (1965) appear as horizontal lines.

Inspection of figure 4 reveals that a satisfactory match between experiment and theory exists for EG1 ≃ 0·1–0·15, and EG2 ≃ 0·1–0·05. Noting the small value of c for these distortions, $c \simeq 0{\cdot}01$ MHz, we conclude that the theory predicts an axially symmetric interaction. This agrees with experiment (Watkins and Corbett 1965) where no deviation from axial symmetry was reported. The computed angle $\delta_1 = 49\,^\circ$ compares favourably with the experimental value of 55·2 °. The interpretation of the data for shell $(\bar{3}, 3, \bar{1})$ is less straightforward. The sensitivity of the calculated results on the distortion parameters, together with the close similarity between the tensors G1 and G2, makes an identification of the $(\bar{3}, 3, \bar{1})$ shell tensor with any of these debatable. Nevertheless, the agreement for G1 is better than for G2. Theory predicts an interaction with only small deviations from axial symmetry, and this only holds for G1. An identification of shell $(\bar{3}, 3, \bar{1})$ with tensor G1 is in conflict with the conclusion based upon motional-averaging experiments (Watkins and Corbett 1965).

3.4. Other relaxation modes

As there is clearly room for improvement, other relaxation modes were also considered.

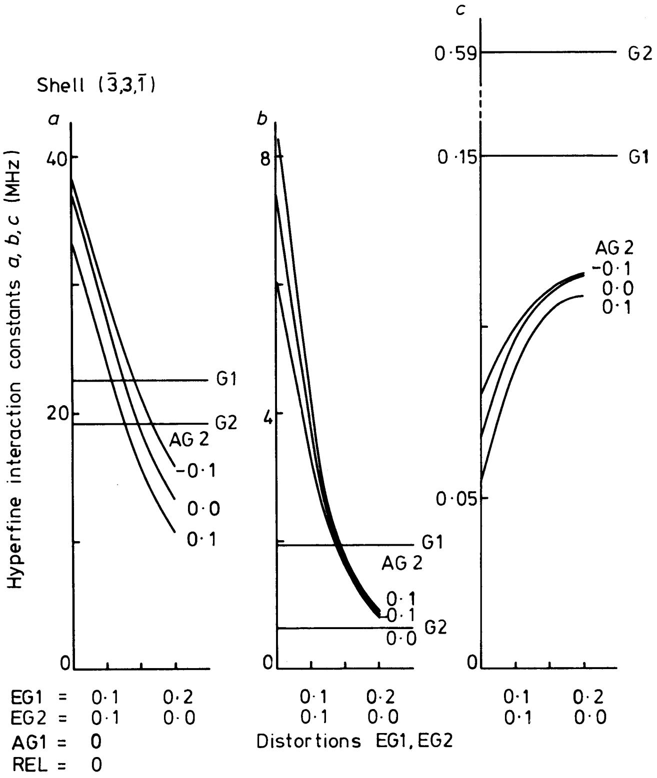

Figure 5. Computed results for the hyperfine interaction constants *a*, *b* and *c* for the nearest-neighbour general class shell ($\bar{3}$, 3, $\bar{1}$) for (EG1, EG2) combinations on the straight line EG1 + EG2 = 0·2. Value of AG2 is label to the curves, AG1 = REL = 0. Experimental values for the tensor components, from De Wit *et al* (1975), are given as horizontal lines.

The first of these are the two symmetric relaxation modes AG1 and AG2, depicted in figure 2. Once the D_{3d} degeneracy has been lifted they are again of importance. Calculations were only performed for AG1 = ±0·1, and AG2 = ±0·1, along the tracks EG1 + EG2 = 0, and EG1 + EG2 = 0·2. Generally, the effects of symmetric relaxation are small. Besides, its effect on the curves representing the best match is like a uniform shift. In particular, the distance between the curves $a(1, 3, 3)$–M1 and $b(1, 3, 3)$–M1 may not be reduced appreciably by these relaxation modes. The dependence of *a*, *b* and *c* on AG2 is larger, in general. This parameter is therefore shown in figures 4 and 5.

The effect of relaxation of the next-nearest-neighbour atoms was also considered. These atoms were displaced in a direction parallel to the displacement vector of the corresponding nearest neighbour, but scaled down in magnitude by a factor of two or four. This is described by the parameter REL = 0·5, REL = 0·25, respectively. For the latter value the new position of the second neighbour is again the centre of gravity of the one first neighbour of the divacancy and the three third neighbours. Second-neighbour relaxation usually has a rather small effect on the hyperfine constants.

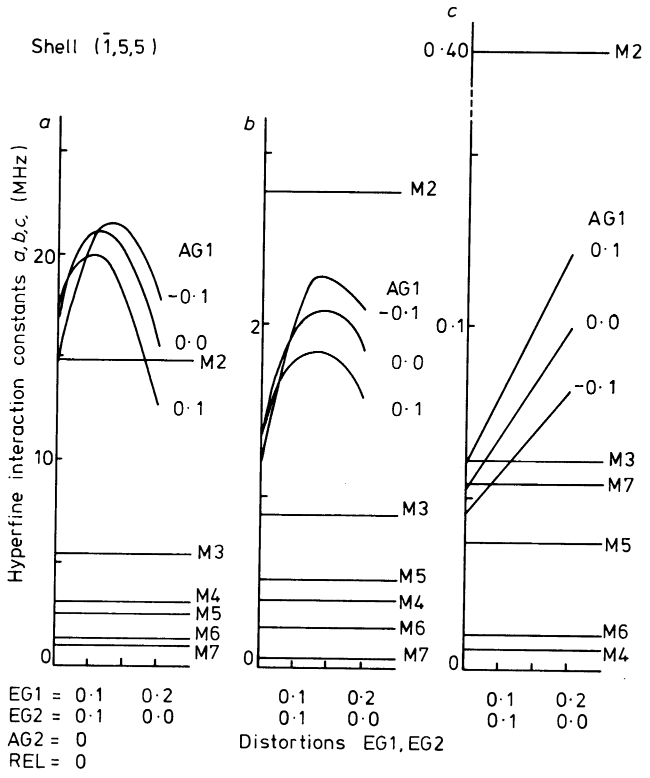

Figure 6. Computed results for the hyperfine interaction constants *a*, *b* and *c* for the second-neighbour mirrorplane class shell (1̄, 5, 5) against the distortion parameters EG1, EG2 and AG1. AG2 = REL = 0. Experimental values from De Wit *et al* (1975).

3.5. Next-nearest-neighbour tensors

The 18 second-neighbour atoms of the divacancy form the (1̄, 5, 5) mirrorplane class shell and four general class shells. For these shells tentative tensor assignments can be made at best. The calculated results for shell (1̄, 5, 5) are shown in figure 6. Though there seems to be reasonable agreement with tensor M2, apart from constant *c*, there is a large discrepancy with regard to the direction of the axis of symmetry. In this respect there is even excellent agreement with tensor M3, which therefore also should be kept as a candidate. As an example of a general class shell of next-nearest-neighbour atoms, and of the effectiveness of the relaxation parameter REL, figure 7 is finally presented. An identification of this shell with tensor G5 might be suggested.

References

De Wit J G, Ammerlaan C A J and Sieverts E G 1975 *Lattice Defects in Semiconductors 1974* (Inst. Phys. Conf. Ser. 23) pp178–84

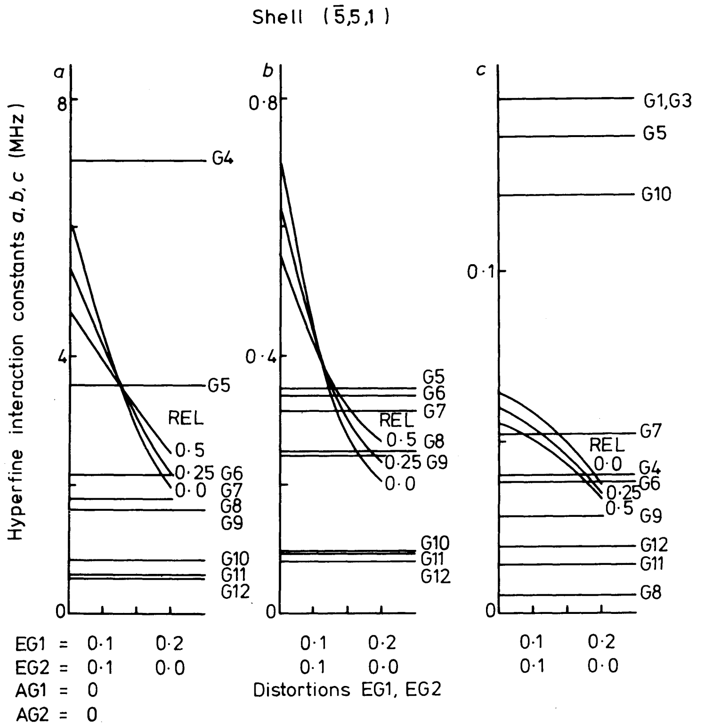

Figure 7. Computed results for the hyperfine interaction constants a, b and c for the second-neighbour general class shell $(\bar{5}, 5, 1)$ against the distortion parameters EG1, EG2, and REL. AG1 = AG2 = 0. Experimental values from De Wit *et al* (1975).

De Wit J G, Sieverts E G and Ammerlaan C A J 1976 *Phys. Rev.* **B14** 3494–503
Hoffmann R 1963 *J. Chem. Phys.* **39** 1397–412
Kwok L Y 1974 *Phys. Stat. Solidi* **B66** 619–26
Lee T F andMcGill T C 1973 *J. Phys. C: Solid St. Phys.* **6** 3438–50
Messmer R P 1975 *Lattice Defects in Semiconductors 1974* (Inst. Phys. Conf. Ser. 23) pp44–55
Messmer R P and Watkins G D 1970 *Phys. Rev. Lett.* **25** 656–9
—— 1973a *Phys. Rev.* **B7** 2568–90
—— 1973b *Radiation Damage and Defects in Semiconductors* (Inst. Phys. Conf. Ser. 16) pp255–61
Watkins G D and Corbett J W 1964 *Phys. Rev.* **134** A1359–77
—— 1965 *Phys. Rev.* **138** A543–55